Monthly Notices of the ROYAL ASTRONOMICAL SOCIETY

MNRAS **438,** 2924–2937 (2014) doi:10.1093/mnras/stt2400
Advance Access publication 2014 January 14

Type Ib SN 1999dn as an example of the thoroughly mixed ejecta of Ib supernovae

Zach Cano,[1⋆] Keiichi Maeda[2,3] and Steve Schulze[4,5]

[1]*Centre for Astrophysics and Cosmology, Science Institute, University of Iceland, Reykjavik 107, Iceland*
[2]*Department of Astronomy, Kyoto University, Kitashirakawa-Oiwake-cho, Sakyo-ku, Kyoto 606-8502, Japan*
[3]*Kavli Institute for the Physics and Mathematics of the Universe (WPI), Todai Institutes for Advanced Study, The University of Tokyo, 5-1-5 Kashiwanoha, Kashiwa, Chiba 277-8583, Japan*
[4]*Instituto de Astrofísica, Facultad de Física, Pontificia Universidad Católica de Chile, Casilla 306, Santiago 22, Chile*
[5]*Millennium Center for Supernova Science, Camino del Observatorio 1515, Las Condes, Chile*

Accepted 2013 December 11. Received 2013 December 7; in original form 2013 August 23

ABSTRACT

We present the results of modelling archival observations of Type Ib SN 1999dn. In the spectra, two He I absorption features are seen: a slower component with larger opacity, and a more rapid He I component with smaller opacity. Complementary results are obtained from modelling the bolometric light curve of SN 1999dn, where a two-zone model (dense inner region, and less dense outer region) provides a much better fit than a one-zone model. A key result we find is that roughly equal amounts of radioactive material are found in both regions. The two-zone analytical model provides a more realistic representation of the structure of the ejecta, including mixing and asymmetries, which offers a physical explanation for how the radioactive material is propelled to, and mixed within, the outer regions. Our result supports the theoretical expectation that the radioactive content in the outflow of a Type Ib supernova (SN) is thoroughly mixed. We fit our model to six additional SNe Ibc, of which the majority of the SNe Ib are best described by the two-zone model, and the majority of the SNe Ic by the one-zone model. Of the SNe Ic, only SN 2007gr was best fitted by the two-zone model, indicating that the lack of helium spectral features for this event cannot be attributed to poor mixing.

Key words: methods: analytical – methods: data analysis – methods: observational – supernovae: general – supernovae: individual: 1999dn.

1 INTRODUCTION

Type Ib and Ic supernovae (SNe) arise from massive stars whose outer envelopes of hydrogen (Ib) and helium (Ic) have been stripped, either partially or completely, before exploding. SNe Ibc are observationally classified by their optical spectra (e.g. Filippenko 1997), where SNe Ib exhibit strong He I lines, while SNe Ic exhibit very weak or no He I lines. The spectra of SNe Ib and Ic have shown that both subclasses are quite heterogeneous, with varying strengths of the He I lines in SNe Ib, and the occasional presence of weak He I lines in the latter. It has thus been suggested by Filippenko (1997) that rather than being distinctly different subclasses, it may be more appropriate to consider that a continuum of helium strengths exist among SNe Ibc, and that the presence or lack of He I lines in the spectra simply reflects the physical conditions within the SN.

Studies have shown that helium lines arise via non-thermal excitation (e.g. Li & McCray 1995; Li, Hillier & Dessart 2012), and require a departure from local thermodynamic equilibrium (LTE; e.g. Harkness et al. 1987; Lucy 1991; Swartz et al. 1993; Dessart et al. 2011). High-energy γ-rays are produced during the radioactive decay of nickel into cobalt and then into iron ($^{56}_{28}\mathrm{Ni} \rightarrow {}^{56}_{27}\mathrm{Co} \rightarrow {}^{56}_{26}\mathrm{Fe}$), which Compton scatter with free and bound electrons, ultimately producing high-energy electrons that deposit their energy in the ejecta through heating, excitation and ionization. Building upon work done by Woosley, Langer & Weaver (1995), recent theoretical models (e.g. Dessart et al. 2011, 2012; Li et al. 2012) have found that while SNe Ic display very weak/no He I lines, this may not be due simply to helium deficiency in SNe Ic, but rather the requirement for producing He I lines is that the nickel is mixed thoroughly enough so that the helium and nickel are within a γ-ray mean free path.

Two schools of thought currently exist regarding the lack of strong helium spectral lines for SNe Ic: either the helium is present but essentially hidden because it is not excited due to poor mixing (Woosley et al. 1995; Dessart et al. 2011, 2012; Li et al. 2012), or simply the helium is not present. However Hachinger et al. (2012) find that only a small amount of helium needs to be present

⋆E-mail: zcano@mail.com

(0.06–0.14 $M_\odot$) to then be observed, implying that it is not possible to hide very much helium in the ejecta. Observations are clearly needed to try and distinguish between these theoretical scenarios.

In fact, He I lines have been observed in some SNe Ic. Type Ic SN 1997B displayed a strong absorption feature in the near-infrared (NIR) that was attributed by Clocchiatti et al. (2004) as due to the He I λ10 830 triplet. Filippenko et al. (1995) found strong, blueshifted He I λ10 830 during the first month post-maximum of SN 1994I. Clocchiatti et al. (1996) presented evidence showing that the centroid of the sodium doublet (λλ5890, 5896, hereafter Na I D) in 1987M and 1994I shifts to the blue a few weeks after maximum, which is likely due to a growing He I λ5876 line blending on the blue side of Na I D absorption feature. However, it was also argued by Wheeler et al. (1994) that the spectra of 1987M and 1994I are also consistent with the complete absence of He I, with much less than 0.1 $M_\odot$ of hydrogen and helium in the ejecta. Finally, Matheson et al. (2001) found no compelling evidence for the presence of helium lines in a large sample of SNe Ic spectra.

Interpreting the absorption feature redward of 10 000 Å in Ibc spectra has proved to be controversial, and it is not completely accepted whether this line is solely due to the He I λ10 830 triplet, whether it is blended with other atoms/ions, or whether it is entirely due to alternative ions. Millard et al. (1999) fit the λ10 250 absorption feature of SN 1994I with a combination of C I λ10 695 and He I λ10 830, with the latter detached at 18 000 km s^{-1}. Gerardy et al. (2002) found that the absorption feature around 10 500 Å for SN 2002ap (Ic-BL; broad-lined Ic) and SN 2000we (Ic) was best fitted by a blend of Mg II, C II and Si I. The same authors did find that the He I triplet was a good fit to the 10 500 Å feature in SN 2001B (Ib). Moreover, Mazzali & Lucy (1998) have also suggested that the λ10 830 absorption feature can be Mg II λ10 910, though this was for Type Ia SN 1994D. It therefore appears that this NIR absorption feature can be due to many atoms and/or ions whose relative contribution varies from event to event.

In this paper, we have attempted to determine the origins of this absorption feature in a Type Ib supernova (SN 1999dn) in a very straightforward manner, and in doing so we have also determined the distribution of the radioactive elements within the ejecta. We make the assumption that the absorption feature redward of 10 000 Å is He I λ10 830, and then calculate its blueshifted velocity. We then look for other He I absorption features at this velocity. If He I absorption features in the visible part of the spectra are seen at this blueshifted velocity, then we regard this as strong evidence that the NIR absorption feature is He I. Here, we have inspected two epochs of spectra taken of Type Ib SN 1999dn by Matheson et al. (2001), which occurred in nearby galaxy NGC 7714. Falco et al. (1999) measured the redshift of NGC 7714, finding $z = 0.009\,35$, which is the value used in this paper.

In Section 2, we search for blueshifted He I lines in both spectra, and then model the first epoch using SYN++ (Thomas, Nugent & Meza 2011). In Section 3, we model the bolometric light curve (LC) of SN 1999dn constructed from the photometry obtained by Benetti et al. (2011) using a one- and two-zone model originally presented in Maeda et al. (2003), to determine the distribution of nickel within the ejecta. We model six additional SNe Ibc and then discuss our results in Section 4, and summarize our conclusions in Section 6.

2 SPECTRA

Spectra of SN 1999dn, originally presented in Matheson et al. (2001), were downloaded from the WiseREP SN spectrum data base (Yaron & Gal-Yam 2012).[1] The two epochs investigated here both display the NIR absorption feature of interest, and are for phases +17 d (1999 September 17) and +38 d (1999 October 08) from *R*-band maximum brightness, using the terminology from Matheson et al. (2001). The spectra have been transformed to rest-frame wavelength, but they have not been corrected for rest-frame extinction.

For both epochs, a single Gaussian was fitted to this absorption feature using a program written in PYXPLOT.[2] While neither spectrum extends far enough into the infrared to show the *entire* absorption feature, in both epochs a clear trough is observed as well as a slight increase in flux at redder wavelengths. This behaviour is more clearly pronounced in the +17 d spectrum, but is still evident in the later epoch.

2.1 +17 d

A single Gaussian (in red) has been fitted to the spectra (Fig. 1) in the range 9800−10 500 Å. The best-fitting parameters of the fit give a central wavelength of $\lambda_{\rm He}$ =10 281 Å, which if this line is due to He I λ10 830, corresponds to a blueshifted velocity of $v_{\rm He} = -15\,576$ km s^{-1}. The solid green lines show He I lines λ4471, λ5876, λ6678, λ7065 and λ7281 moving at −8500 km s^{-1}, while the dashed red lines are the same He I features moving at −15 600 km s^{-1}.

In the +17 d spectrum, clear absorption features are seen at ∼6400 Å and ∼6700 Å, which are likely due to blueshifted He I λ6678 and λ7065 at the (larger) velocity determined from the Gaussian fit. A weak feature blueward of the He I λ5876 feature at −8500 km s^{-1} is also seen, which is likely due to the same He I line but at −15 600 km s^{-1}.

While a clear absorption feature is seen for He I λ4471 at −8500 km s^{-1}, no corresponding absorption feature is seen at −15 600 km s^{-1}, which is likely due to it being blended with strong Fe II and Ti II lines. It is also seen that the blueshifted absorption line of He I λ7281 at −15 600 km s^{-1} is likely blended (on the red side) with the He I λ7065 line at −8500 km s^{-1}.

2.2 +38 d

At +38 d, the same weak He I absorption features are seen in Fig. 2 at the higher velocity determined from the Gaussian fit. This time the central wavelength is found to be $\lambda_{\rm He} = 10\,339$ Å, which if this line is due to He I λ10 830, corresponds to a blueshifted velocity of $v_{\rm He} = -13\,909$ km s^{-1}. The central wavelength has moved to the redder part of the spectrum, indicating that the velocity has decreased between the two epochs.

The same two absorption features at ∼6400 Å and ∼6700 Å that were seen in the +17 d spectrum are still there, and their velocity is consistent with that determined from the Gaussian fit, although the feature at ∼6700 Å is better fitted by a slightly higher velocity of ∼ −15 500 km s^{-1}. Another absorption feature is seen at ∼5600 Å, which may be due to blueshifted He I λ5876 at −13 909 km s^{-1}.

In conclusion, in both epochs two helium components are seen in the spectra: one corresponding to the stronger, and slower moving He I lines, and another higher velocity component that is consistent with the velocity determined from the Gaussian fit of the absorption feature redward of 10 000 Å.

[1] http://www.weizmann.ac.il/astrophysics/wiserep/
[2] http://pyxplot.org.uk

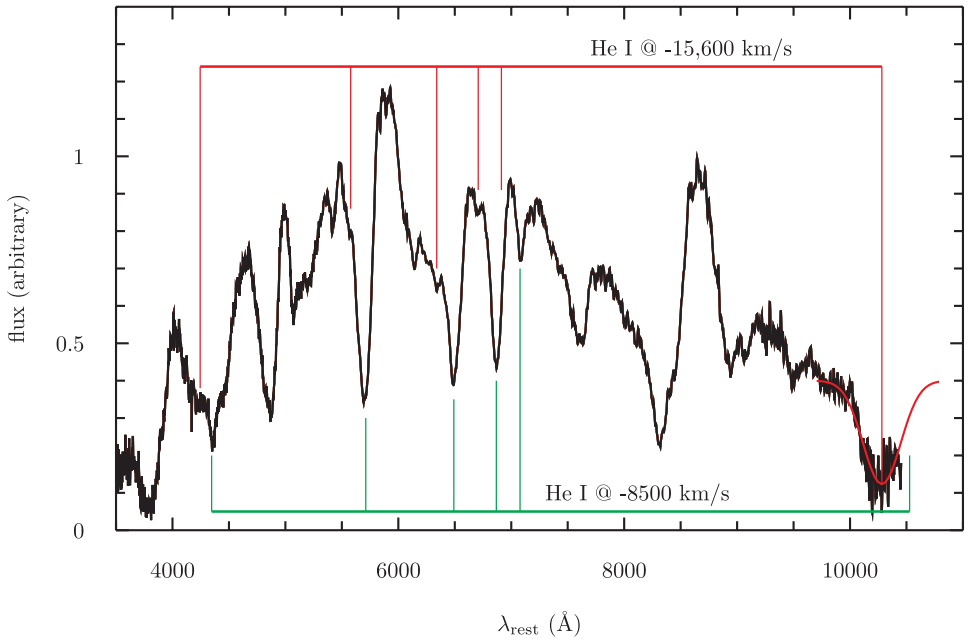

Figure 1. Rest-frame spectrum of SN 1999dn (Ib) at +17 d (1999 September 17), obtained by Matheson et al. (2001). A single Gaussian (in red) has been fitted to the spectra in the range 9800–10 500 Å. The best-fitting parameters of the fit give a central wavelength of 10 281 Å, which if this line is due to He I λ10 830, corresponds to a velocity of $v_{\rm He} = -15\,576\,{\rm km\,s^{-1}}$. The green lines show He I lines λ4471, λ5876, λ6678, λ7065 and λ7281 moving at $-8500\,{\rm km\,s^{-1}}$, while the red lines are the same He I features moving at $-15\,576\,{\rm km\,s^{-1}}$. Two absorption features are seen at ∼6400 Å and ∼6700 Å, which may be due to blueshifted He I λ6678 and λ7065 at the (higher) velocity determined from the Gaussian fit. A weak feature blueward of the He I λ5876 feature at $-8500\,{\rm km\,s^{-1}}$ is also seen, which is likely due to the same He I line but at $-15\,600\,{\rm km\,s^{-1}}$, and it is also seen that the blueshifted absorption line of He I λ7281 at $-15\,600\,{\rm km\,s^{-1}}$ is likely blended (on the red side) with the He I λ7065 line at $-8500\,{\rm km\,s^{-1}}$.

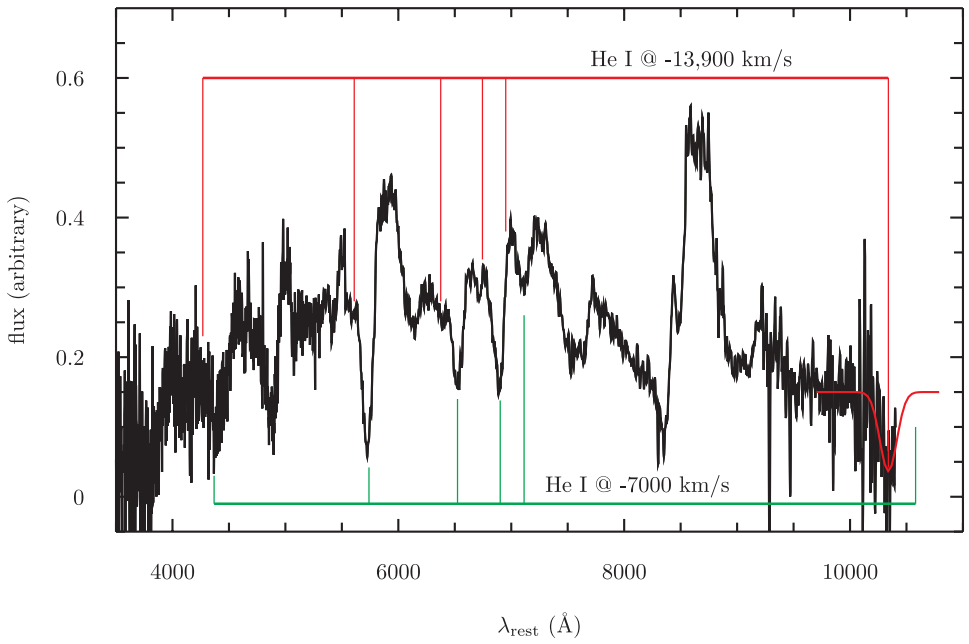

Figure 2. Rest-frame spectrum of SN 1999dn (Ib) at +38 d (1999 October 08), obtained by Matheson et al. (2001). A single Gaussian (in red) has been fitted to the spectra in the range 9800–10 500 Å. The best-fitting parameters of the fit give a central wavelength of 10 339 Å, which if this line is due to He I λ10 830, corresponds to a velocity of $v_{\rm He} = -13\,909\,{\rm km\,s^{-1}}$. The solid green lines are the same He I lines as in Fig. 1, but this time moving at $-7000\,{\rm km\,s^{-1}}$, while the red lines are the same He I features moving at $-13\,909\,{\rm km\,s^{-1}}$. The ejecta velocities have clearly decreased between the two epochs. The same two absorption features at ∼6400 Å and ∼6700 Å that were seen in the +17 d spectrum are still there, and their velocity is consistent with that determined from the Gaussian fit, although the feature at ∼6700 Å is better fit by a slightly higher velocity of $\sim -15\,500\,{\rm km\,s^{-1}}$. An additional absorption feature is seen at ∼5600 Å, which may be due to blueshifted He I λ5876.

2.3 Spectral modelling

The investigation presented in the previous sections has shown that there is a strong possibility that there are two velocity components for He I in the spectra of SN 1999dn. Next, we modelled the spectrum from +17 d with SYN++ to see if we can reproduce the He I features at the two velocities. As mentioned in the previous section, we have not corrected for rest-frame extinction, which has a small value ($E(B-V)_{\rm rest} = 0.048$ mag) and will not affect the SYN++ fit significantly.

Plotted in Fig. 3 are two synthetic spectra, one with a single He I component fit at a blueshifted velocity of $-8500\,{\rm km\,s^{-1}}$ (green), which is detached from the photospheric velocity of $v_{\rm phot} = 6000\,{\rm km\,s^{-1}}$, and the other with an additional velocity component, also detached, at $-15\,600\,{\rm km\,s^{-1}}$ (red). In the SYN++ modelling, the velocity of the higher velocity component is restricted to the range 15 600–20 000 km s^{-1}. The photospheric velocity and blackbody temperature ($T_{\rm bb} = 5000$ K) are identical in both model spectra. With regards to the modelling parameters, both spectra are identical apart from the inclusion of a second He I component in the red spectrum. The rest of the lines in the spectra are due to Fe II, O I, Ca II, Ti II and Si II. The Sobolev opacity of the He I line at the slower(faster) velocities are $\log(\tau) = 0.4(-0.4)$, which is computed using a strong reference line (for He I is λ7771.94 Å) that the other He I lines are normalized against. In this simple model, the opacity of the slower component is higher than that of the more rapid component.

It is seen that the spectrum that includes a second, higher velocity He I component reproduces the weak absorption lines around 6400 and 6700 Å, which are due to blueshifed He I λ6678 and λ7065 at $-15\,600\,{\rm km\,s^{-1}}$, and are not present in the single-component model. It is seen that the synthetic blueshifted He I λ5876 absorption feature in the two-component model is much stronger than the actual spectrum, and is probably a blend of blueshifted He I at $-15\,600\,{\rm km\,s^{-1}}$ and Fe II at the photospheric velocity. We also note that SYN++ assumes LTE level populations whereas He I lines are non-thermally excited. It is therefore not unexpected that the He I fluxes are not correctly reproduced. In particular, the 2s3s stare is metastable, and hence, λ10 830 will have a much larger optical depth than, for example, λ5876. Finally, no absorption feature is seen for blueshifted He I λ4471 in the two-component synthetic spectrum which agrees with the results from Section 2.

Branch et al. (2002) performed an in-depth analysis of the +17 d spectrum of SN 1999dn. Using SYNOW, they found a good fit to the spectrum using $v_{\rm phot} = 6000\,{\rm km\,s^{-1}}$ and $T_{\rm bb} = 4800$ K, and the same elements listed above. In their spectrum, He I was detached at $-8000\,{\rm km\,s^{-1}}$, which is a close match to the velocity determined here for the slower He I component. Encouragingly, they also predict a blueshifted He I λ10 830 line at $-8000\,{\rm km\,s^{-1}}$ with their SYNOW model (see fig. 3 in Branch et al. 2002).

Additionally, Deng et al. (2000) modelled low-resolution spectra of SN 1999dn at three epochs, the last one being 1999 September 14 (i.e. three days before the epoch modelled here). Using SYNOW, they found $v_{\rm phot} = 9000\,{\rm km\,s^{-1}}$ and $T_{\rm bb} = 5300$ K, which are consistent with the parameters derived here and by Branch et al. (2002). However, unlike our study, Deng et al. (2000) have included many more atoms and ions in their modelling: in addition to those listed above, they also used Mg II, [O II], C I, C II, Na I, Ca I, Ni II and H I.

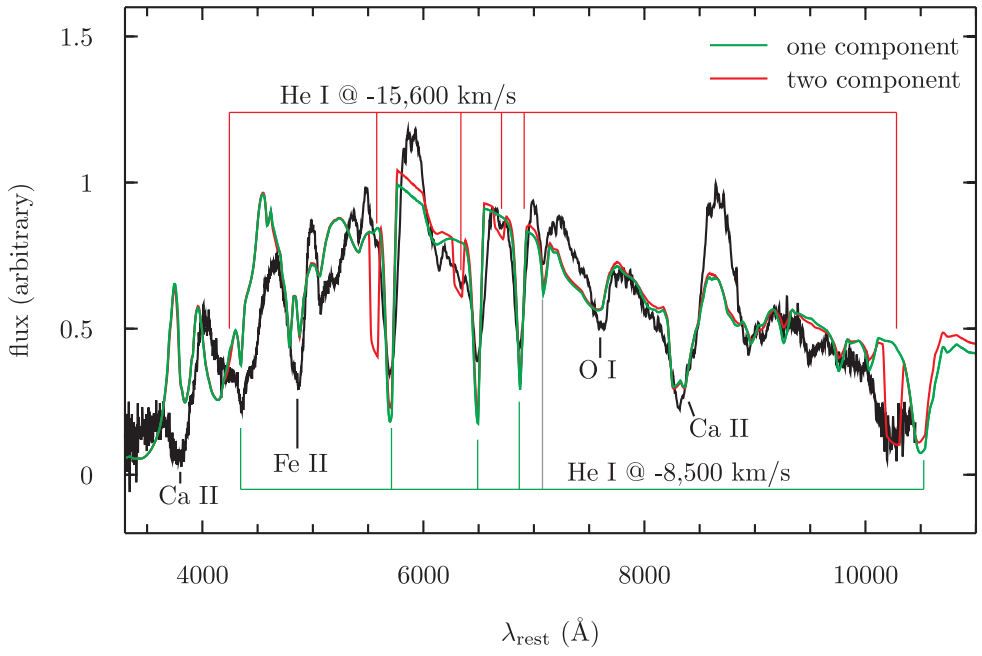

Figure 3. Rest-frame spectrum of SN 1999dn (Ib) at +17 d obtained by Matheson et al. (2001), which has been modelled with synthetic spectra created with SYN++. The blackbody temperature is $T_{\rm bb} = 5000$ K and the photospheric velocity is $v_{\rm phot} = 6000\,{\rm km\,s^{-1}}$. Two synthetic spectra are shown, one with only a single He I component at a velocity of $-8500\,{\rm km\,s^{-1}}$ (green), and another with two velocity components at $-8500\,{\rm km\,s^{-1}}$ and $-15\,600\,{\rm km\,s^{-1}}$ (red). All other atoms/ions (Fe II, O I, Ca II, Ti II) are at the photospheric velocity. The two-component synthetic spectrum reproduces the weak absorption lines around 6400 and 6700 Å, which are due to blueshifted He I λ6678 and λ7065 at $-15\,600\,{\rm km\,s^{-1}}$. These lines are not present in the single-component model. Note that the two-component model overpredicts the absorption line at blueshifted He I λ5876, which is a combination of He I and Fe II. The opacity of the higher velocity He I component in the two-component model is lower than the slower component, which is the same as in the bolometric modelling, where the inner, slower component also has a higher opacity than the outer, quicker component. All atoms/ions are labelled in the figure, apart from Ti II, which accounts for line-blanketing at wavelengths blueward of 6000 Å.

Interestingly, Deng et al. (2000) have also questioned whether two different C II velocity components exist in the helium layer, with the ions detached at $-20\,000\,\mathrm{km\,s^{-1}}$ at early times, and at roughly $-10\,000\,\mathrm{km\,s^{-1}}$ on September 14. However, the authors favour a different scenario in which the absorption feature near 6300 Å is due to Hα in the early epochs, at $\sim -19\,000\,\mathrm{km\,s^{-1}}$, while in September 14 epoch the same feature is C II (6580 Å), thus concluding that a thin high-velocity hydrogen layer exits outside of the slower helium layer in SN 1999dn.

The results of the SYN++ modelling generally reproduce the results seen in the preceding section, namely that it is likely that there are two components of He I in the outflow of SN 1999dn. The clearest evidence arises from the blueshifted He I features at $-15\,600\,\mathrm{km\,s^{-1}}$, especially blueshifted He I λ6678 and λ7065, which are only present in the two-component model.

3 BOLOMETRICS

3.1 Time of explosion

By comparing the rise time of SN 1999dn with those of other SNe Ibc, Benetti et al. (2011) estimated the date of explosion to have occurred ≈1999 August 16 (JD = 245 1406.0).

Using equation 17 of Piro & Nakar (2013), it is possible to put a lower limit on the explosion date by using a measurement of the photospheric velocity and temperature at a single epoch during the LC rise. Benetti et al. (2011) modelled several epochs of spectroscopy obtained of 1999dn using SYNOW, with two epochs occurring before maximum light (−6.0 and −2.3 d). Using their results from −2.3 d (JD = 245 1415.7): $T_{\rm bb} \sim 9100\,\mathrm{K}$, $v_{\rm phot} \sim 10\,400\,\mathrm{km\,s^{-1}}$ and the luminosity determined from our bolometric LC ($L \sim 1.05 \times 10^{42}$ erg s^{-1}), we find $t_{\rm min} = 5.1$ d. This implies a lower limit to the explosion date of JD = 245 1410.6, or ≈1999 August 20.

We have also used the results from the spectrum modelled by Benetti et al. (2011) for the epoch −6 d (JD = 245 1413.5): $T_{\rm bb} \sim 7000\,\mathrm{K}$, $v_{\rm phot} \sim 15\,000\,\mathrm{km\,s^{-1}}$. We have estimated the luminosity at this epoch (which extend further back in time than our actual bolometric LC) by fitting a t^2 curve (Arnett 1982) to the early bolometric LC, and then extracting the luminosity at JD = 245 1413.5, to which we find $L \sim 8.4 \times 10^{41}$ erg s^{-1}. This implies $t_{\rm min} = 5.3$ d before this measurement, and a lower limit to the explosion date of JD = 245 1408.2, which is ≈1999 August 17. This epoch predicts an earlier limit to the date of explosion compared with the latter epoch, and within two days of the explosion date estimated by Benetti et al. (2011). Taking into consideration the results of Benetti et al. (2011) and those found here, throughout this paper we have used an explosion date of JD = 245 1408.0 ± 2.0 d.

3.2 Construction of the bolometric LC

We collected the photometry published by Benetti et al. (2011), and using their value of the total extinction along the line of site ($E(B-V)_{\rm total} = 0.10 \pm 0.05$ mag) created a quasi-bolometric LC in filters *UBVRI*. While the bulk of radiation emitted by a given SN is emitted primarily in the optical bands, work by e.g. Tomita et al. (2006), Modjaz et al. (2009) and Cano et al. (2011) have shown that roughly 50–70 per cent of the radiation is emitted within *UBVRI*, with a sizeable contribution early on in the UV, and an increasing contribution in the IR well after the peak. Therefore, our derived bolometric LC may have a large systematic uncertainty of the order of ∼20 per cent. We note that due to the paucity of IR observations of SN 1999dn, as well as a desire to keep the analysis as simple as possible without introducing additional sources of uncertainty, we have not attempted to estimate the IR contribution as we have done for other work (e.g. Cano et al. 2011).

Our general procedure for creating the bolometric LC (as well as those presented in Section 4.2) is as follows.

(i) Collect published *UBVRI* photometry.
(ii) Correct for extinction along the entire line of sight (foreground and rest frame).
(iii) Convert magnitudes into monochromatic fluxes using flux zero-points in Fukugita, Shimasaku & Ichikawa (1995).
(iv) For each epoch of multiband observations (i.e. for each spectral energy distribution, SED), using the effective wavelengths from Fukugita et al. (1995):

(i) Interpolate (linearly) between each data point.
(ii) Integrate the SED over frequency, assuming zero flux at the integration limits.
(iii) Correct for 'filter overlap'.

The linear interpolation and integration were performed using a program written in PYXPLOT. In order to make the most of the published photometry, when there was an epoch without contemporaneous *UBVRI* photometry, we interpolated the individual LCs (using a linear interpolation) to estimate the amount of 'missing' flux in a given filter. The resulting fluxes in units (mJy Hz) are converted into units of (erg s^{-1} m^{-2}), and then into luminosities using the distances derived from the observed redshifts which were calculated using the latest cosmological parameters determined by *Planck* [Ade et al. (Planck Collaboration) 2013; $H_0 = 67.3\,\mathrm{km\,s^{-1}\,Mpc^{-1}}$, $\Omega_{\rm M} = 0.315$ $\Omega_\Lambda = 0.685$].

Peak bolometric light was determined using a program written in PYTHON that fits multi-order polynomials to the bolometric LC. The best-fitting parameters are found using scipy.optimize.leastsq, which minimizes the sum of squares to the fitted polynomial. The peak time is then found using scipy.optimize.fmin to find the minimum of the function, which in this case is the negative of the fitted polynomial. The program was then run several times over different time ranges (i.e. excluding arbitrarily chosen data points) to determine the statistical uncertainty of the derived peak time. The total error in the peak time is therefore a combination of the uncertainty in the explosion date as well as the statistical uncertainty from the fit, which we have added in quadrature.

Taking the date of explosion to be JD = 245 1408.0 ± 2.0 d, we find a peak time of $t_{\rm peak} = 10.14 \pm 2.04$ d. The luminosity at peak light is found to be $L_{\rm peak} = 1.13 \times 10^{42}$ erg s^{-1}.

3.3 One-zone model

Using an adaptation of the Arnett (1982) model, which includes the energy produced by the decay of nickel into cobalt, and then into iron, we have estimated the mass of nickel nucleosynthesized during the explosion to be $M_{\rm Ni} = 0.040 \pm 0.005\,\mathrm{M_\odot}$. The uncertainty in the nickel mass is statistical only, and is dominated primarily by the uncertainty in the explosion date. The median nickel mass determined by Cano (2013) for an SN Ib is $M_{\rm Ni} = 0.16\,\mathrm{M_\odot}$ (though over a larger frequency interval, and includes IR photometry); thus, it appears that SN 1999dn synthesized much less nickel than the 'typical' SN Ib.

As the bolometric LC extends to over 115 d, we attempted to constrain the nickel mass from the exponential tail using a simple one-zone model (Maeda et al. 2003, M03 hereon). M03 investigated

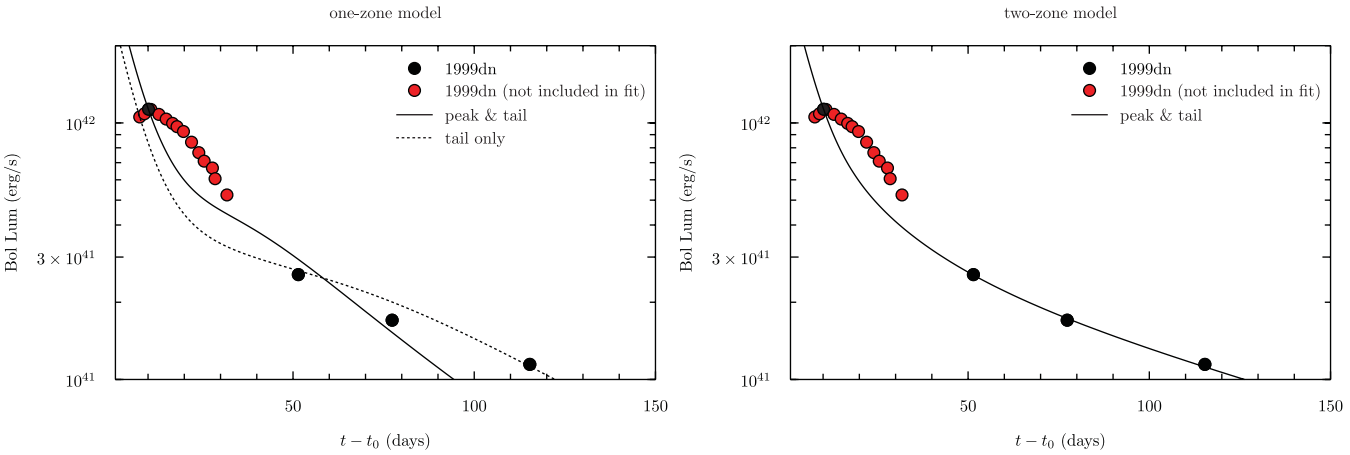

Figure 4. Bolometric LC of SN 1999dn. *Left:* the peak+tail (solid) and tail (dotted) have been fitted with the one-zone model from Maeda et al. (2003) for all data at times >50 d. For the one-zone model to be deemed a good fit to the bolometric LC, the nickel mass found from fitting the peak+tail must be approximately the same as that from fitting only the tail. It is found that the nickel mass and opacity found from fitting just the tail do not provide a good fit to the peak+tail data ($R^2 = 0.748$), which is also reflected by the fact that the dotted line does not dissect the peak of the LC. It is also seen that the solid line in the one-zone model does not reproduce the tail very well. Instead, the two-zone model (*right*) provides a much better fit to the peak+tail, both visually and statistically ($R^2 = 0.998$). The nickel masses and opacities found from fitting both models are displayed in Table 1.

the issue of γ-ray transport in SN ejecta using a simple model, building upon work done previously by Clocchiatti & Wheeler (1997). The decay of nickel into cobalt, and then into iron produces γ-rays and positrons, of which a fraction of the former are thermalized and deposit their energy into the SN ejecta. As with the Arnett model, we have included the energy deposited by the decay of nickel and cobalt into their daughter products:

$$L(t) = M_{\rm Ni}(\mathrm{e}^{-t/t_{\rm Co}}[\epsilon_{\rm Co}(1-\mathrm{e}^{-\tau}) + \epsilon_{e^+}]) \quad (1)$$

and

$$L(t) = M_{\rm Ni}(\mathrm{e}^{-t/t_{\rm Ni}}[\epsilon_{\rm Ni}(1-\mathrm{e}^{-\tau})]), \quad (2)$$

where time t is expressed in units of days, $t_{\rm Co}$ is the e-folding time of ^{56}Co (113 d; M03) and $M_{\rm Ni}$ is the mass of nickel produced during the explosion in units of grams. $\tau = \kappa_\gamma \rho R = \tau_0/t^2$ is the optical depth to γ-rays, where τ_0 is the optical depth to γ-rays at $t = 1$ d. The energy input from γ-rays and positrons are $\epsilon_\gamma = 6.8 \times 10^9$ erg s^{-1} g^{-1} and $\epsilon_{e^+} = 2.4 \times 10^8$ erg s^{-1} g^{-1}, respectively. Positron channels are negligible for the decay of nickel into cobalt, so this term does not appear in equation (2). We have also assumed that the same optical depth applies to both decay reactions, though in reality the optical depths for $^{56}_{28}\mathrm{Ni} \rightarrow {}^{56}_{27}\mathrm{Co}$, and $^{56}_{27}\mathrm{Co} \rightarrow {}^{56}_{26}\mathrm{Fe}$ differ due to the different line energies of the emitted γ-rays; however, given the large optical depth early on this effect should be negligible. By adding equations (1) and (2) and then fitting them to the bolometric LC, it is possible to determine the amount of nickel nucleosynthesized during the explosion, where $M_{\rm Ni}$ and τ_0 are the free parameters during the fit.

When performing the fit, we are interested in obtaining a good fit to the bolometric peak as well as the late-time tail. The phase between the peak and the tail, which we will refer to as the 'slope', is less important when fitting the data because during this period energy that was trapped before the peak is still being released as the photosphere recedes into the ejecta, and the SN expands, decreasing the overall optical depth. Therefore, it is expected that the luminosity predicted by our single-zone model is less than the observations. It should be considered however that this model should be able to successfully recover the peak luminosity from fitting of only the tail phase.

A key uncertainty then is determining when the 'slope' phase transitions into the 'tail' phase. As such, we have fitted the bolometric LC of SN 1999dn at $t - t_0 > 50$ and 60 d with a PYTHON program that uses scipy.optimize.leastsq to find the best-fitting parameters for each model. Our fitting procedure is to fit: (1) the peak[3]+tail simultaneously to determine $M_{\rm Ni}$ and τ_0, (2) just the tail to determine $M_{\rm Ni}$ and τ_0, and then compare.

For the one-zone model to be considered a good fit to the bolometric LC, the nickel masses found from fitting just the tail must be similar to that found from fitting the peak+tail. This is because even though the fit obtained from fitting the peak+tail may appear to be a good statistical fit to the data, the tail can be poorly reproduced (e.g. Fig. 4 on the left). From a theoretical standpoint, it is important to obtain a very good fit to the slope in order to reproduce the exact amount of nickel created during the explosion.

For each fit, we have estimated the goodness of fit by calculating the correlation coefficient, R^2, for: (1) the peak+tail simultaneously, (2) just the tail and (3) the peak+tail using the fitted values determined from fitting just the tail. Thus, if the values obtained from fitting just the tail are a good match to those from fitting the peak+tail, the correlation coefficient will reflect this as a good statistical fit. We have estimated the errors in the best-fitting parameters by performing the fit several times to account for the uncertainty in the date of explosion. As such we have modelled three bolometric LCs of SN 1999dn, each with a different date of explosion (i.e. the minimum, maximum and exact date of explosion). We then calculated the average value of each parameter, and used the spread of values as an indication of the statistical error derived from the fit. Our results are listed in Table 1, and the models are displayed in Fig. 4.

What becomes quickly apparent is that the nickel mass obtained from fitting just the tail ($M_{\rm Ni} = 0.024 - 0.030\,\mathrm{M}_\odot$) is less than that obtained from fitting the peak+tail simultaneously ($M_{\rm Ni} = 0.041\,\mathrm{M}_\odot$), and for which we recover the nickel mass obtained from the Arnett model. It is also seen that the value of R^2 calculated from fitting the peak+tail when using the nickel mass

[3] This is the fiducial peak determined from our PYTHON program.

Table 1. Best-fitting parameters from the one- and two-zone models.

SN	Type	Model	Fitted Parameters	+40 d	R^2	+50 d	R^2	+60 d	R^2	1 or 2 zones
1999dn	Ib	One-zone: p+t	$M_{\rm Ni}$ ($M_\odot$)	–	–	0.041 ± 0.007	0.993 (all)	0.041 ± 0.007	0.998 (all)	–
–	–	–	τ_0	–	–	4360 ± 1100	–	6260 ± 1260	–	–
–	–	One-zone: t only	$M_{\rm Ni}$ ($M_\odot$)	–	–	0.030 ± 0.002	0.748 (all)	0.024 ± 0.001	0.603 (all)	**2**
–	–	–	τ_0	–	–	18100 ± 450	0.956 (t)	38000 ± 1300	1.000 (t)	–
–	–	Two-zone:p+t	$M_{\rm Ni,\,in}$ ($M_\odot$)	–	–	0.019 ± 0.000	1.000 (all)	–	–	–
–	–	–	$M_{\rm Ni,\,out}$ ($M_\odot$)	–	–	0.021 ± 0.007	–	–	–	–
–	–	–	$\tau_{0,\rm in}$	–	–	404000 ± 80000	–	–	–	–
–	–	–	$\tau_{0,\rm out}$	–	–	1400 ± 350	–	–	–	–
–	–	Arnett	$M_{\rm Ni}$ ($M_\odot$)	0.040 ± 0.005		–	–	–	–	–
–	–	–	–	–	–	–	–	–	–	–
2007Y	Ib	One-zone: p+t	$M_{\rm Ni}$ ($M_\odot$)	0.042 ± 0.007	0.999 (all)	0.042 ± 0.004	1.000 (all)	0.039 ± 0.011	1.000 (all)	–
–	–	–	τ_0	780 ± 80	–	850 ± 15	–	1700 ± 900	–	–
–	–	One-zone: t only	$M_{\rm Ni}$ ($M_\odot$)	0.020 ± 0.000	0.663 (all)	0.048 ± 0.003	0.987 (all)	0.007 ± 0.041	0.020 (all)	**Uncertain**
–	–	–	τ_0	2660 ± 20	0.996 (t)	710 ± 30	1.000 (t)	25000 ± 24350	1.000 (t)	–
–	–	Two-zone:p+t	$M_{\rm Ni,\,in}$ ($M_\odot$)	0.006 ± 0.002	0.999 (all)	0.004 ± 0.018	1.000 (all)	≈ 0.042	1.000 (all)	–
–	–	–	$M_{\rm Ni,\,out}$ ($M_\odot$)	0.067 ± 0.016	–	0.042 ± 0.024	–	≈ 0.006	–	–
–	–	–	$\tau_{0,\rm in}$	4500 ± 870	–	3750 ± 2900	–	≈ 730	–	–
–	–	–	$\tau_{0,\rm out}$	210 ± 10	–	350 ± 290	–	≈ 910	–	–
–	–	Arnett	$M_{\rm Ni}$ ($M_\odot$)	0.034 ± 0.003	–	–	–	–	–	–
–	–	–	–	–	–	–	–	–	–	–
2008D	Ib	One-zone: p+t	$M_{\rm Ni}$ ($M_\odot$)	≈ 0.047	0.989 (all)	≈ 0.047	0.994 (all)	≈ 0.047	0.999 (all)	–
–	–	–	τ_0	≈ 1900	–	≈ 2150	–	≈ 2460	–	–
–	–	One-zone: t only	$M_{\rm Ni}$ ($M_\odot$)	≈ 0.031	0.753 (all)	≈ 0.025	0.558 (all)	≈ 0.025	0.557 (all)	**2**
–	–	–	τ_0	≈ 4800	0.971 (t)	≈ 7950	0.992 (t)	≈ 7760	0.982 (t)	–
–	–	Two-zone:p+t	$M_{\rm Ni,\,in}$ ($M_\odot$)	≈ 0.012	1.000 (all)	≈ 0.017	1.000 (all)	≈ 0.009	–	–
–	–	–	$M_{\rm Ni,\,out}$ ($M_\odot$)	≈ 0.036	–	≈ 0.089	–	≈ 0.038	–	–
–	–	–	$\tau_{0,\rm in}$	≈ 21000	–	≈ 9100	–	≈ 162000	–	–
–	–	–	$\tau_{0,\rm out}$	≈ 1000	–	≈ 120	–	≈ 1450	–	–
–	–	Arnett	$M_{\rm Ni}$ ($M_\odot$)	0.039 ± 0.001	–	–	–	–	–	–
–	–	–	–	–	–	–	–	–	–	–
2009jf	Ib	One-zone: p+t	$M_{\rm Ni}$ ($M_\odot$)	0.166 ± 0.007	0.975 (all)	0.165 ± 0.008	0.979 (all)	0.163 ± 0.007	0.989 (all)	–
–	–	–	τ_0	1640 ± 20	–	1810 ± 115	–	2300 ± 190	–	–
–	–	One-zone: t only	$M_{\rm Ni}$ ($M_\odot$)	0.108 ± 0.029	0.812 (all)	0.072 ± 0.005	0.479 (all)	0.064 ± 0.003	0.387 (all)	**2**
–	–	–	τ_0	3600 ± 1160	0.924 (t)	11700 ± 2200	0.951 (t)	17800 ± 1200	0.996 (t)	–
–	–	Two-zone:p+t	$M_{\rm Ni,\,in}$ ($M_\odot$)	0.030 ± 0.005	0.996 (all)	0.038 ± 0.001	1.000 (all)	0.032 ± 0.002	–	–
–	–	–	$M_{\rm Ni,\,out}$ ($M_\odot$)	0.151 ± 0.011	–	0.185 ± 0.018	–	0.516 ± 0.075	–	–
–	–	–	$\tau_{0,\rm in}$	$4e6 \pm 0.2e6$	–	$0.12e6 \pm 1.1e6$	–	27700 ± 6500	–	–
–	–	–	$\tau_{0,\rm out}$	940 ± 130	–	500 ± 10	–	120 ± 65	–	–
–	–	Arnett	$M_{\rm Ni}$ ($M_\odot$)	0.138 ± 0.010	–	–	–	–	–	–
–	–	–	–	–	–	–	–	–	–	–
2004aw	Ic	One-zone: p+t	$M_{\rm Ni}$ ($M_\odot$)	0.080 ± 0.022	0.995 (all)	0.080 ± 0.023	0.996 (all)	0.081 ± 0.021	0.999 (all)	–
–	–	–	τ_0	5100 ± 1800	–	5100 ± 1600	–	6050 ± 2020	–	–
–	–	One-zone: t only	$M_{\rm Ni}$ ($M_\odot$)	0.076 ± 0.014	0.990 (all)	0.064 ± 0.008	0.932 (all)	0.057 ± 0.007	0.865 (all)	**1**
–	–	–	τ_0	6150 ± 1600	0.967 (t)	11500 ± 2850	0.992 (all)	30400 ± 16350	0.996 (t)	–
–	–	Two-zone:p+t	$M_{\rm Ni,\,in}$ ($M_\odot$)	0.032 ± 0.002	0.998 (all)	0.045 ± 0.006	1.000 (all)	0.052 ± 0.006	–	–
–	–	–	$M_{\rm Ni,\,out}$ ($M_\odot$)	0.048 ± 0.025	–	0.035 ± 0.029	–	0.028 ± 0.029	–	–
–	–	–	$\tau_{0,\rm in}$	56800 ± 6000	–	40900 ± 8440	–	35250 ± 6000	–	–
–	–	–	$\tau_{0,\rm out}$	3250 ± 1000	–	1950 ± 220	–	820 ± 400	–	–
–	–	Arnett	$M_{\rm Ni}$ ($M_\odot$)	0.077 ± 0.011	–	–	–	–	–	–
–	–	–	–	–	–	–	–	–	–	–
2007gr	Ic	One-zone: p+t	$M_{\rm Ni}$ ($M_\odot$)	0.029 ± 0.006	0.961 (all)	0.029 ± 0.006	0.979 (all)	0.029 ± 0.006	0.990 (all)	–
–	–	–	τ_0	1600 ± 300	–	2000 ± 400	–	2500 ± 550	–	–
–	–	One-zone: t only	$M_{\rm Ni}$ ($M_\odot$)	0.013 ± 0.001	0.570 (all)	0.012 ± 0.000	0.510 (all)	0.012 ± 0.000	0.491 (all)	**2**
–	–	–	τ_0	13500 ± 950	0.975 (t)	17800 ± 60	0.992 (t)	19750 ± 125	0.994 (t)	–
–	–	Two-zone:p+t	$M_{\rm Ni,\,in}$ ($M_\odot$)	0.009 ± 0.001	1.000 (all)	0.009 ± 0.002	1.000 (all)	0.008 ± 0.001	–	–
–	–	–	$M_{\rm Ni,\,out}$ ($M_\odot$)	0.021 ± 0.013	–	0.022 ± 0.081	–	0.021 ± 0.015	–	–
–	–	–	$\tau_{0,\rm in}$	26000 ± 1400	–	24200 ± 7200	–	28600 ± 3100	–	–
–	–	–	$\tau_{0,\rm out}$	430 ± 100	–	360 ± 300	–	590 ± 300	–	–
–	–	Arnett	$M_{\rm Ni}$ ($M_\odot$)	0.026 ± 0.003	–	–	–	–	–	–
–	–	–	–	–	–	–	–	–	–	–
2011bm	Ic	One-zone: p+t	$M_{\rm Ni}$ ($M_\odot$)	0.368 ± 0.008	0.991 (all)	0.361 ± 0.009	0.987 (all)	0.369 ± 0.004	0.991 (all)	–
–	–	–	τ_0	6967 ± 144	–	7250 ± 100	–	7200 ± 120	–	–
–	–	One-zone: t only	$M_{\rm Ni}$ ($M_\odot$)	0.364 ± 0.008	0.991 (all)	0.333 ± 0.007	0.973 (all)	0.318 ± 0.002	0.951 (all)	**1**
–	–	–	τ_0	7150 ± 175	0.989 (t)	8892 ± 188	0.987 (t)	9950 ± 560	0.985 (t)	–
–	–	Two-zone:p+t	$M_{\rm Ni,\,in}$ ($M_\odot$)	0.090 ± 0.000	0.998 (all)	0.095 ± 0.000	0.997 (all)	0.088 ± 0.012	0.998 (all)	–
–	–	–	$M_{\rm Ni,\,out}$ ($M_\odot$)	0.292 ± 0.009	–	0.281 ± 0.010	–	0.288 ± 0.003	–	–
–	–	–	$\tau_{0,\rm in}$	395000 ± 17000	–	$6.46e6 \pm 4.45e6$	–	$0.49e6 \pm 1.94e6$	–	–
–	–	–	$\tau_{0,\rm out}$	4740 ± 130	–	4760 ± 100	–	5000 ± 275	–	–
–	–	Arnett	$M_{\rm Ni}$ ($M_\odot$)	0.349 ± 0.022	–	–	–	–	–	–

Notes. The value of the correlation coefficient for the one-zone model is insensitive to the actual slope of the tail, whose precise value is necessary for determining the nickel mass. Therefore, a good statistical fit to the one-zone model does not imply that an accurate nickel mass has been obtained. For the one-zone model to be deemed a good fit (e.g. SN 2004aw), the nickel mass determined from fitting the tail should be close to that from fitting the peak+tail, which is then reflected as a high R^2 value when the tail values are fit on to the peak+tail. The boldface has been used to draw attention to the best fitting model for each supernova.

and optical depth obtained from fitting just the tail are much lower than those determined from the other fits, while inspection of Fig. 4 (left) shows the poor visual fit of the tail when the one-zone model is fitted to the tail+peak simultaneously. This behaviour is consistently found over both time-ranges. This leads us to conclude that the single-zone model provides a poor physical description of the configuration of the ejecta.

3.4 Two-zone model

The single-zone model of M03 is an approximation that considers a single homogeneous sphere with a constant density. However, in reality the geometry of many SNe may not be perfectly symmetric. One solution can be to consider a homogeneous bipolar cone with an opening angle θ. Another solution is the one proposed by M03: a simple one-dimensional (1D) model that approximates the configuration of the ejecta to be in two regions. In a 1D explosion, most of the material is expelled at a high velocity, leaving a central, low-velocity region at quite low density. This is seen especially for cases where the kinetic energy is large, such as those measured for hypernovae ($E_{\rm ke} > 10^{52}$ erg). As such, 1D models are only able to account for the total inflow/outflow in a single direction. 2D and 3D explosions are not limited by this however, where it is possible to have an inflow and outflow simultaneously with different velocities. The consequence of this is a central region with a higher density/optical depth than is possible in simple 1D explosion models, and an outer region of smaller density/optical depth. Thus, the two-zone model provides a measure of the amount of mixing occurring in the ejecta, as well as including a degree of the asymmetry in the explosion, both of which are consistent with hydrodynamic models of strongly jetted explosions (e.g. Maeda & Nomoto 2003).

The energy deposited in the ejecta by γ-rays and positrons from the decay of cobalt into iron then becomes

$$L(t) = M_{\rm Ni,in}{\rm e}^{-t/t_{\rm Co}}[\epsilon_{\rm Co}(1-{\rm e}^{-\tau_{\rm in}})+\epsilon_{e^+}] + M_{\rm Ni,out}{\rm e}^{-t/t_{\rm Co}}[\epsilon_{\rm Co}(1-{\rm e}^{-\tau_{\rm out}})+\epsilon_{e^+}], \quad (3)$$

where the variables have the same meaning as in equation (1), but this time we consider two deposits of ^{56}Ni (an inner and an outer). The energy deposited by the decay of nickel into cobalt in the two zones can be similarly approximated as in Section 3.3 but without the positron contribution. Both contributions are then added together and then fitted to the bolometric LC, for which there are now four free parameters: $M_{\rm Ni,\,in}$, $M_{\rm Ni,\,out}$, $\tau_{0,\,\rm in}$ and $\tau_{0,\,\rm out}$.

We fit the two-zone model to the bolometric LC of SN 1999dn for $t - t_0 > 50$ d, but due to more free parameters than data points we were not able to fit for $t - t_0 > 60$ d. Here, we find the total nickel mass ejected, $M_{\rm Ni,\,total} = M_{\rm Ni,\,in} + M_{\rm Ni,\,out} = 0.040 \pm 0.008\,{\rm M}_\odot$, which agrees with that determined from the one-zone model (for peak+tail) and the Arnett model. It is also seen that the opacity of the inner region ($\tau_{0,\,\rm in} = 404\,000 \pm 80\,000$) is much higher than the outer region ($\tau_{0,\,\rm out} = 1400 \pm 350$), with values that are similar to seen from fitting the hypernovae in M03. Here, the quoted errors are statistical, and arise predominantly from the uncertainty in the explosion date.

Some exciting conclusions may be drawn from our results: (1) the outflow of SN 1999dn is better fitted by the two-zone model, implying that the ejecta is likely asymmetric, and (2) similar amounts of nickel are found in the inner ($M_{\rm Ni,\,in} = 0.019\,{\rm M}_\odot$) and outer ($M_{\rm Ni,\,out} = 0.021\,{\rm M}_\odot$ regions, implying that the outer regions of the ejecta are thoroughly mixed with radioactive material. Encouragingly, a similar result was observed by Takaki et al. (2013) for Ib SN 2012au who also fitted their bolometric LC with the two-zone model of M03, finding nickel masses in the inner and outer regions of 0.14 and 0.12 $\rm M_\odot$, respectively.

4 DISCUSSION

4.1 Helium lines

When analysing the spectra of SN 1999dn, He I absorption lines were seen at two velocities: a slower velocity at which the stronger He I lines were seen, and a larger velocity that was determined by attributing the NIR absorption feature as being due to He I λ10 830, and fitting a Gaussian to it to determine its blueshifted velocity. With regards to the on-going debate about the origin of this spectral feature it appears, at least in this event, that it is only He I at a larger blueshifted velocity than the stronger He I lines. Support for this conclusion comes from the fact that multiple He I lines are seen at the larger velocity in the optical, with the same lines appearing consistently in both epochs. It is seen that the blueshifted velocity of the λ10 830 absorption feature decreased between the two epochs, falling from $-15\,576\,{\rm km\,s^{-1}}$ at 17 past maximum light to $-13\,909\,{\rm km\,s^{-1}}$ 21 d later.

Deng et al. (2000) modelled three epochs of spectra of SN 1999dn, with their last epoch being three days younger than the epoch modelled here. Deng et al. (2000) also concluded that the SN outflow has different velocity components, with a slower helium layer and a more rapid hydrogen layer. This independent analysis supports the idea that the ejecta is not a single homogeneous blob expanding homologously, but rather is comprised of regions moving with different velocities.

4.2 Two-zone model applied to other SNe Ibc

The results from fitting the two-zone model to the bolometric LC of SN 1999dn showed that similar amounts of nickel/cobalt are present in the inner and outer regions of the ejecta. If we take our results at face value, they imply that the amount of mixing is at least partially due to the ejecta having an asymmetric structure. Therefore, in the case of SN 1999dn, the presence of helium spectral lines can be explained by the ejecta being well mixed and the nickel and helium are located in close proximity in the ejecta.

One wonders however how much can we trust these results when applied to only a single event. Certainly, other authors such as Takaki et al. (2013) have found similar results for another Type Ib SN (2012au), but what about other SNe Ibc? And what about the outstanding uncertainty about the unknown role of mixing in SNe Ib versus Ic? Do all SNe Ibc contain similar amounts of helium in the ejecta, but only appear in the spectra of SNe Ib due to mixing brought about via asymmetric explosions?

In an attempt to address these questions, we have modelled three additional SNe Ib (SNe 2007Y, 2008D, 2009jf) and three SNe Ic (SNe 2004aw, 2007gr, 2011bm) using the one- and two-zone models. We chose these particular SNe from the sampled presented in Cano (2013) as both foreground and rest-frame extinction were known, and more crucially, observations of these SNe extended well into the tail phase, therefore making them suitable to be modelled. The bolometric LCs were constructed using the procedure described in Section 3.2, and we have also determined the time of peak bolometric light for each SNe using our PYTHON program and the explosion dates published in the literature. Table 2 lists the literature references for the photometry, redshifts, total extinction along the line of sight and our derived peak times and luminosities.

Table 2. Photometry references.

SN	Type	z	$E(B-V)_{\rm total}$	$t_{\rm peak}$ (d)	$L_{\rm peak}$ (erg s^{-1})	Refs.
1999dn	Ib	0.009 38	0.100	10.14 ± 2.04	1.13×10^{42}	(1),(2)
2007Y	Ib	0.004 657	0.102	18.35 ± 1.51	0.61×10^{42}	(3)
2008D	Ib	0.007	0.622	18.00 ± 0.46^a	0.76×10^{42}	(4)
2009jf	Ib	0.007 942	0.113	21.44 ± 1.07	2.25×10^{42}	(5)
2004aw	Ic	0.0175	0.364	10.01 ± 2.99	2.24×10^{42}	(6)
2007gr	Ic	0.001 728	0.090	12.28 ± 2.50	0.67×10^{42}	(7)
2011bm	Ic	0.0221	0.064	31.26 ± 1.50	4.12×10^{42}	(8)

[a]The exact explosion time is known, therefore the quoted error arises only from the statistical uncertainty from determining the peak.
References: (1) Matheson et al. (2001); (2) Benetti et al. (2011); (3) Stritzinger et al. (2009); (4) Malesani et al. (2009); (5) Valenti et al. (2011); (6) Taubenberger et al. (2006); (7) Hunter et al. (2009); (8) Valenti et al. (2012).

We have modelled the SNe using the procedure in Sections 3.3 and 3.4, where due to the abundance of data points for the chosen SNe, we have fitted the bolometric LCs over three ranges: $t - t_0 > 40$, 50 and 60 d. As before, the telling statistic to elucidate the best-fitting model is the value of R^2 from fitting the peak+tail using the nickel mass and opacity determined from fitting only the tail in the single-zone model. Table 1 displays the best-fitting values from the two models.

4.2.1 SN 2007Y (Ib)

Neither the one- nor two-zone modelling consistently proved to be the preferred model for SN 2007Y. For all three time ranges, the one-zone model consistently determined that $\approx$0.04–0.05 $M_\odot$ of nickel was synthesized, which is slightly more than that predicted by the Arnett model ($M_{\rm Ni} = 0.034 \pm 0.003\,M_\odot$). However, for times >40 and 60 d the value of the correlation coefficient was quite low when the nickel mass and opacity determined from fitting only the tail in the one-zone model were then applied to the peak+tail in the one-zone model. At >40 d the total nickel mass determined from the two-zone model was much greater than that for the single-zone model, though at >60 d the nickel masses closely agreed. At >50 d the one-zone model fits the data very well, with the nickel mass determined from fitting the peak+tail and just the tail in the one-zone model agreeing closely.

4.2.2 SN 2008D (Ib)

The results for SN 2008D are much more conclusive, and indicate that the bolometric LC is best fitted by the two-zone model. The nickel masses derived from the one- and two-zone models agree well ($M_{\rm Ni} \approx 0.047\,M_\odot$), which is slightly more than that determined from the Arnett model ($M_{\rm Ni} = 0.039 \pm 0.001\,M_\odot$). For all three time-ranges, the nickel mass derived from fitting the tail only in the one-zone model was much less than that from fitting the peak+tail, and the value of R^2 calculated for fitting the peak+tail using the values from fitting just the tail indicated that the one-zone model was a poor fit, which can also be seen visually.

The total nickel mass determined from the two-zone model for >50 d ($M_{\rm Ni} = 0.107 \pm 0.001\,M_\odot$) was much greater than that found in the one-zone model. For times >40 and 60 d, the total nickel mass was approximately the same as determined from the one-zone model, with both indicating that roughly 3–4 times more nickel is present in the outer layers compared with the inner.

4.2.3 SN 2009jf (Ib)

The bolometric LC of SN 2009jf is best fitted by the two-zone model; however, the results from all three time ranges are not as consistent as for some of the other SNe. The nickel masses derived from the one- and two-zone models agree well ($M_{\rm Ni} = \approx 0.163-0.166\,M_\odot$), which is slightly more than that determined from the Arnett model ($M_{\rm Ni} = 0.138 \pm 0.010\,M_\odot$). For times >40 d, the one-zone model could be argued to be a suitable fit to the data; however, the one-zone model was a poor fit for the other time ranges. The total nickel mass derived from the two-zone model for >60 d is 3 times larger than for any other model, indicating that the one- and two-zone models are both poor fits to the data for times >60 d. Moreover, the optical depth of the inner region is very high, $\tau_{0,\rm in} = (0.1-4) \times 10^6$, much higher than is seen for the other SNe for which the two-zone model was the better fit. This may be indicating that the ejecta of SN 2009jf is complicated and may possess more than two zones. However, if we take the results of the two-zone model at face value, it then suggests that on average $\approx$5 times more nickel is present in the outer layers relative to the inner, denser region.

4.2.4 SN 2004aw (Ic)

For SN 2004aw, the nickel mass and opacity determined from fitting the tail only in the one-zone model, and then applied to the peak+tail provides a good visual and statistical fit for all three time ranges. Both the one- and two-zone models estimate that $\approx 0.08\,M_\odot$ of nickel was created during the explosion, which agrees well with that determined from the Arnett model ($M_{\rm Ni} = 0.077 \pm 0.011\,M_\odot$). The one-zone model provides a good, consistent fit to the bolometric LC of SN 2004aw.

4.2.5 SN 2007gr (Ic)

For all three time ranges, the one-zone model was a poor fit, and the bolometric LC of SN 2007gr is best fitted by the two-zone model. Both models predict that $\approx 0.03\,M_\odot$ of nickel was nucleosynthesized during the explosion, which agrees well with the nickel mass derived from the Arnett model ($M_{\rm Ni} = 0.026 \pm 0.003\,M_\odot$). The value of R^2 determined by fitting the peak+tail with the values obtained from fitting just the tail in the one-zone model also indicates that the one-zone model is a poor fit, which can also be seen visually. The two-zone model finds that between 2 and 3 times more nickel is found in the outer layers relative to the inner region.

4.2.6 SN 2011bm (Ic)

As for SN 2004aw, the bolometric LC of SN 2011bm is well described by the one-zone model. For all three time ranges, the nickel mass and opacity determined from fitting just the tail in the one-zone model proved to be a good fit for the peak+tail in the one-zone model. All models estimate that $\approx$0.361–0.369 $M_\odot$ of nickel was synthesized during the explosion, which is only slightly higher than the nickel mass found from the Arnett model ($M_{\rm Ni} = 0.349 \pm 0.022\,M_\odot$).

4.2.7 General trends

Some really interesting conclusions can be drawn from the results. First, from a phenomenological perspective, of the SNe Ib, arguably three out of four are best fitted by the two-zone model. The geometry of SN 2007Y proved more difficult to constrain, with the best-fitting model perhaps being the one-zone model, though this model did not consistently prove to be the best fit to the bolometric LC over all three time ranges. That the bulk of the SNe Ib are fitted by the two-zone model implies that these events have aspherical geometries. Of the SNe Ic, two are best fitted by a one-zone model (SNe 2004aw and 2011bm), while SN 2007gr is better fitted by the two-zone model. In this small sample, two-thirds of the SNe Ic possess spherical symmetry. For SN 2007gr, it appears that the lack of helium spectral features cannot be attributed to poor mixing as the fits over all three time-spans indicate that 2–3 times more nickel are present in the outer layers of the ejecta.

From the modelling, as was seen for SN 1999dn, while the value of the correlation coefficient was seen to be quite good for the one-zone model for all of the SNe, visually the tails of SNe 2008D, 2009jf and 2007gr were poorly reproduced. This is reflected in the much smaller nickel masses estimated from fitting only the tails for these events. Next, the nickel masses determined from the various models were sometimes more than that found using the Arnett model, which suggests that the ratio of peak bolometric to radioactive luminosities is not unity, but may be slightly higher (e.g. Takaki et al. 2013). And finally, for all of the SNe whose bolometric LCs were better described by the two-zone model, the inner region always had a higher opacity to γ-rays than the outer region (see Table 1).

4.3 Amount of nickel mixing

The results of the bolometric modelling allow us to comment on the role of mixing in SNe Ibc. As discussed in the Introduction, the lack of He I lines in Ic spectra may either be due to the absence of helium in the ejecta, or that the helium is present but not excited, therefore making it essentially hidden to the observer.

A very interesting paper by Frey, Fryer & Young (2013) has recently presented results of new convection algorithms that are based not on mixing length theory but instead use 3D hydrodynamics as a guide to model stellar mixing. For stellar progenitor models of SNe Ibc of masses in the range 15–27 $M_\odot$, they showed that enhanced convection may lead to a severe depletion of the helium layers, leaving behind only a thin helium shell comprised primarily of heavier elements. This work suggests that the helium is not observed simply because it is not present the star at the time of explosion.

In stars that have retained some helium before exploding, Dessart et al. (2012, D12 hereon) showed that the nickel needs to be close enough to the helium (i.e. within a γ-ray mean free path) so it is then excited. Thus, for Ibc ejecta of similar helium abundances, ejecta where the nickel/cobalt is more thoroughly mixed will be an SN Ib, while ejecta that is weakly mixed, or strongly asymmetric (including a jet structure), will be an Ic.

For the majority of the SNe Ib modelled here, the best-fitting values from the two-zone model indicate that on average between 2 and 5 times more nickel is present in the outer regions compared with the inner. These values are reminiscent of those found for the hypernovae modelled by M03, indicating that the geometry of SNe Ib possesses a degree of asymmetry. Two of the three SNe Ic bolometric LCs were adequately described by the one-zone model, while the bolometric LC of SN 2007gr was best fitted by the two-zone model, with 2–3 times more nickel in the outer layers. Thus, for SN 2007gr the lack of helium lines cannot be accredited to poor mixing, and is likely due to the absence of helium in the ejecta. It is then tempting to suggest that for the other two SNe Ic the lack of helium lines is due to poor mixing, possibly arising to them having a more spherically symmetric geometry. Certainly, IR helium lines were observed by Taubenberger et al. (2006) for SN 2004aw, both the He λ10 830 and λ20 580 lines, indicating that some helium is present in the ejecta. However, the strong absorption features near λ10 830 in the spectra of SN 2011bm (Valenti et al. 2012) can be explained by C I (λ10,827 Å), which is also the case for SN 2007gr (Valenti et al. 2008). Additionally, neither SN 2011bm nor SN 2007gr show evidence for a He I λ20 580 line. Thus, it appears that no helium is present in the ejecta of SN 2007gr and SN 2011bm, but *is* present for SN 2004aw, implying that the latter is an Ic due to poor mixing. Conversely, one is also drawn to conclude that should helium have been present in the ejecta of SN 2007gr, there may have been enough asphericity, and in turn sufficient mixing present, for this event to have been a Type Ib.

Similarly for the majority of the SNe Ib in our sample the two-zone model was found to be a better fit to the data than the one-zone model. This suggests that they possess an aspherical geometry, and the classification of Ib arises from the close proximity of helium and nickel in the ejecta (i.e. is thoroughly mixed). Though we are not attempting to draw global conclusions based on a modest sample of events, our preliminary analysis implies that a large number of SNe Ib likely possess an aspherical geometry. Studies of nebular spectra of SNe Ibc (Modjaz et al. 2008; Maeda et al. 2008; Taubenberger et al. 2009), in particular the double-peaked [O I] $\lambda\lambda$6300,6363 line, have also drawn the conclusion that a very high fraction of SNe Ibc arise from aspherical explosions, with only a small fraction having lines that were best fitted by a single Gaussian (as opposed to a double-peak profile, or profiles that displayed varying degrees of asphericity). In the sample of 39 SNe Ibc investigated by Taubenberger et al. (2009), only two SNe Ib were best fitted by a single Gaussian, and for both of these events the spectra were of low S/N, making their best-fitting model of these two events somewhat tentative. It is very interesting to note that the bulk of the SNe whose lines were best fitted by a single Gaussian (i.e. possess spherical symmetry) were predominantly of Type Ic.

The last question that begs answering then is how can so much nickel/cobalt be in the outer layers of the ejecta. What does this result imply for the explosion mechanism? The classification of the SNe Ib in our sample is unambiguous – there are clear helium lines in the spectra analysed by several different authors. As noted by D12, to ensure a observational classification of Ib, the 'right' amount of mixing needs to occur in order that the helium in the ejecta undergoes non-thermal excitation. This then restricts the explosion physics through the efficiency of the mixing in the outflow, where even moderately mixed models fail to non-thermally excite helium atoms. Mixing in SN ejecta out to large radii can

arise via different mechanisms which are fundamentally dependent on multidimensional effects (D12). Large-scale mixing can occur due to a jet, large asymmetries in the explosion itself brought about by hydrodynamic instabilities, or via the magnetorotational mechanism (see D12 and references therein), while small-scale mixing can occur that is associated with convection and Rayleigh–Taylor and Kelvin–Helmholtz instabilities. The models of D12 that successfully created SNe Ib involved the explosion of low-mass helium cores in which efficient small-scale mixing occurs, and for which there is only a small oxygen-rich mass boundary between the nickel and the outer layers that are helium rich. As most of the SNe Ib, as well as Type Ic SN 2007gr, are best described by the two-zone model, which is a 1D approximation to 3D asymmetry, the amount of mixing in these events, as well as the mechanism to propel the nickel to the outer layers, can be attributed to the asymmetrical geometry of the outflow.

Finally, while mixing is important for producing helium features in SNe Ib and a lack of these features in some SNe Ic can be attributed to a lack of extensive mixing, there are also cases (e.g. SN 2007gr) where the Ic classification is more likely to arise from the absence of helium in the ejecta. As also surmised by previous authors (e.g. Filippenko 1997), there is likely to be variation in the helium content in the progenitor's envelope, which is influenced by pre-explosion circumstances. All massive stars lose mass during their short lifetimes, where both single and binary stars will lose mass via line-driven winds, the rate of which is highly dependent on the metal content of the star (massive stars of higher metal content lose more mass than those of lower metallicity). This situation is also complicated by the very likely role of binarity in the progenitor stars of SNe Ibc. Observationally, there is compelling research showing that massive stars preferentially occur in binary systems (e.g. Sana et al. 2012), and it has been suggested by several authors (e.g. Podsiadlowski, Joss & Hsu 1992; Smartt 2009; Eldridge et al. 2013) that binaries may be the dominant progenitor route for SNe Ibc. Binary interaction offers a natural way for a star to be stripped of its outer envelope, which in addition to stellar winds, offers a way for the outer layers of the pre-explosion star to be deficient in hydrogen and/or helium.

5 CAVEATS

Two important caveats must be considered. The first is regarding interpreting the very late-time behaviour of the bolometric LCs, especially in those cases where only a few data points are available. It is possible that SNe Ibc may have material surrounding them that was ejected by the progenitor prior to exploding, either episodically, by stellar winds or perhaps ejection during a common-envelope phase. The time-resolved glowing circumstellar rings around SN 1987A (e.g. Panagia et al. 1991) are a prime example, which is also brilliantly illustrated in fig. 1 of Leibundgut & Suntzeff (2003), where the *V*-band ring brightness is 2–3 mag brighter than the ejecta emission. It is not possible to spatially resolve the different emission regions for events occurring in distant galaxies; thus, there may be the danger of interpreting late-time emission generated by the interaction of the SN ejecta with pre-SN ejecta, and not arising from the SN ejecta itself. It is worth pointing out therefore that in this work we have assumed that emission observed at all times arises solely from the SN ejecta.

The second caveat concerns our analytical models. Essentially, the LC fitting consists of two regimes. At the bolometric peak, the luminosity is assumed to be equal to the instantaneous energy deposition rate, which is an approximation that arises from analytical modelling but is also seen in numerical simulations. At later times the luminosity is also assumed to equal the instantaneous energy deposition rate but corrected for the escape of γ-rays into space. While both fitting regions make this assumption, the physics underpinning this assumption are very different.

Deviations from the instantaneous energy deposition rate have been seen in simulations (e.g. Ensman & Woosley 1988; Moriya et al. 2010; Bersten et al. 2012), including the recent models of Dessart et al. (2011, their fig. 13) where the peak luminosity of their simulated SNe Ibc exceed the instantaneous deposition by 0.1–0.3 dex due to 'trapped' radiation diffusing to the surface of the ejecta. In these cases, the *actual* mass of nickel present in the ejecta is *less* than that is assumed from the instantaneous deposition rate, and any attempt to fit a simple analytical model to the bolometric peak will end up overestimating the total amount of nickel in the ejecta. However, deviation from the instantaneous deposition rate will be less during the exponential tail regime as the optical depth in this phase is much less.

In our procedure, we first fit every SN with the one-zone model and tried to match the peak bolometric luminosity with the tail. In several cases, we found that the model luminosity at the tail phase was underpredicted (e.g. SN 2009jf, bottom left of Fig. 5), leading us to add an additional component to the model in order for it to match the observations. Including diffusion effects in the one-zone model will lead to a reduction in the amount of ^{56}Ni in the model, which in turn will decrease the predicted tail luminosity. A reduction in the tail luminosity highlights the need for an additional component in the model, but with even more ^{56}Ni required in the outer zone to fit the observations.

The opposite effect can, in principle, also happen. If an SN is best fitted by the one-zone model but the luminosity at a given epoch exceeds the instantaneous deposition rate, an additional component may be required to explain the observations. However, we are not able to envision a reason why this effect should happen to just SNe Ib or Ic but not both, implying that our general conclusions are not fundamentally changed.

6 CONCLUSIONS

(i) There are two He I components in the optical and NIR spectra of Type Ib SN 1999dn. High-velocity He I lines are seen in both epochs considered here, and their blueshifted velocity decreases between the two epochs.

(ii) Both the spectral and bolometric modelling indicate that the outflow of SN 1999dn has at least two components: an inner region of slower velocity and higher density, and an outer region of higher velocity and lower density.

(iii) The bolometric LC of SN 1999dn is best described by the two-zone model, with roughly equal amounts of nickel in both regions ($\approx$0.02 $M_\odot$). The two-zone model allows us to approximately model 2D or 3D asymmetry and mixing with a 1D model. Thus, the likely asymmetric structure of SN 1999dn provides a physical explanation for how the radioactive material is propelled to, and mixed within, the outer regions of the ejecta.

(iv) We fit the bolometric LCs of six additional SNe Ibc (three Ib and three Ic). Of the seven SNe modelled, four are best described by the two-zone model (three Ib and one Ic), two by the one-zone model (two Ic) and one is uncertain (Ib).

(v) Of the SNe Ic, only SN 2007gr was best fitted by the two-zone model, indicating that for this SN Ic, the lack of helium spectral features cannot be ascribed to poor mixing.

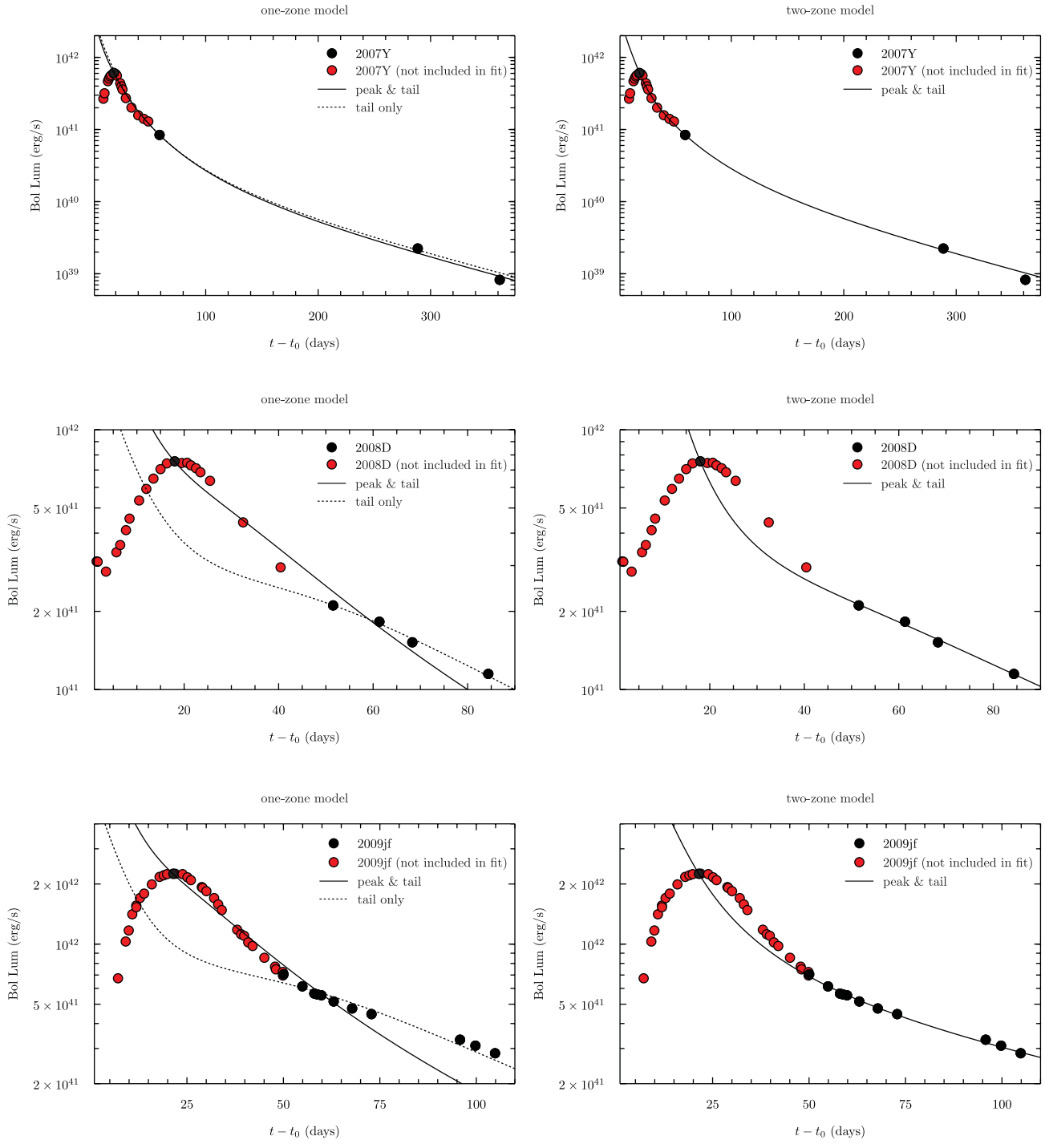

Figure 5. Bolometric LCs of the other SNe Ib in our sample (2007Y, 2008D and 2009jf). The LCs and models are displayed in the same fashion as Fig. 4, with the one-zone models on the left and the two-zone models on the right. The results shown are for times >50 d. *Top:* SN 2007Y. The best-fitting model is uncertain, with the one-zone model providing a good fit for all data >50 d, but the two-zone model being a marginally better fit for times >40 and 60 d. *Middle:* SN 2008D. The best-fitting model is the two-zone model, which estimates that roughly 3–4 times more nickel is found in the outer layers of the ejecta. *Bottom:* SN 2009jf. The best-fitting model is the two-zone model, which finds that almost five times more nickel is present in the outer regions of the ejecta. When fitting the one-zone model to the peak+tail for SNe 2008D and 2009jf, visually the tail is poorly fit. The two-zone model provides a better fit to the bolometric LCs of three of the four SNe Ib considered in this paper, and the best-fitting parameters determined from both models are displayed in Table 1.

Our approach has used observations to address the debate regarding the presence/absence of helium in the ejecta of SNe Ibc, however uncertainties still persist. As such we encourage IR spectroscopic observations of future SNe Ibc in order to help solve this puzzle. Detecting He I λ10 830 is not trivial as this line is often blended with other atoms and ions; however, He I λ20 580 does not suffer such blending. Detection of these lines, coupled with modelling such as that presented here can help determine whether a SN Ic is a Ic due to poor mixing, or due to the absence of helium in the ejecta.

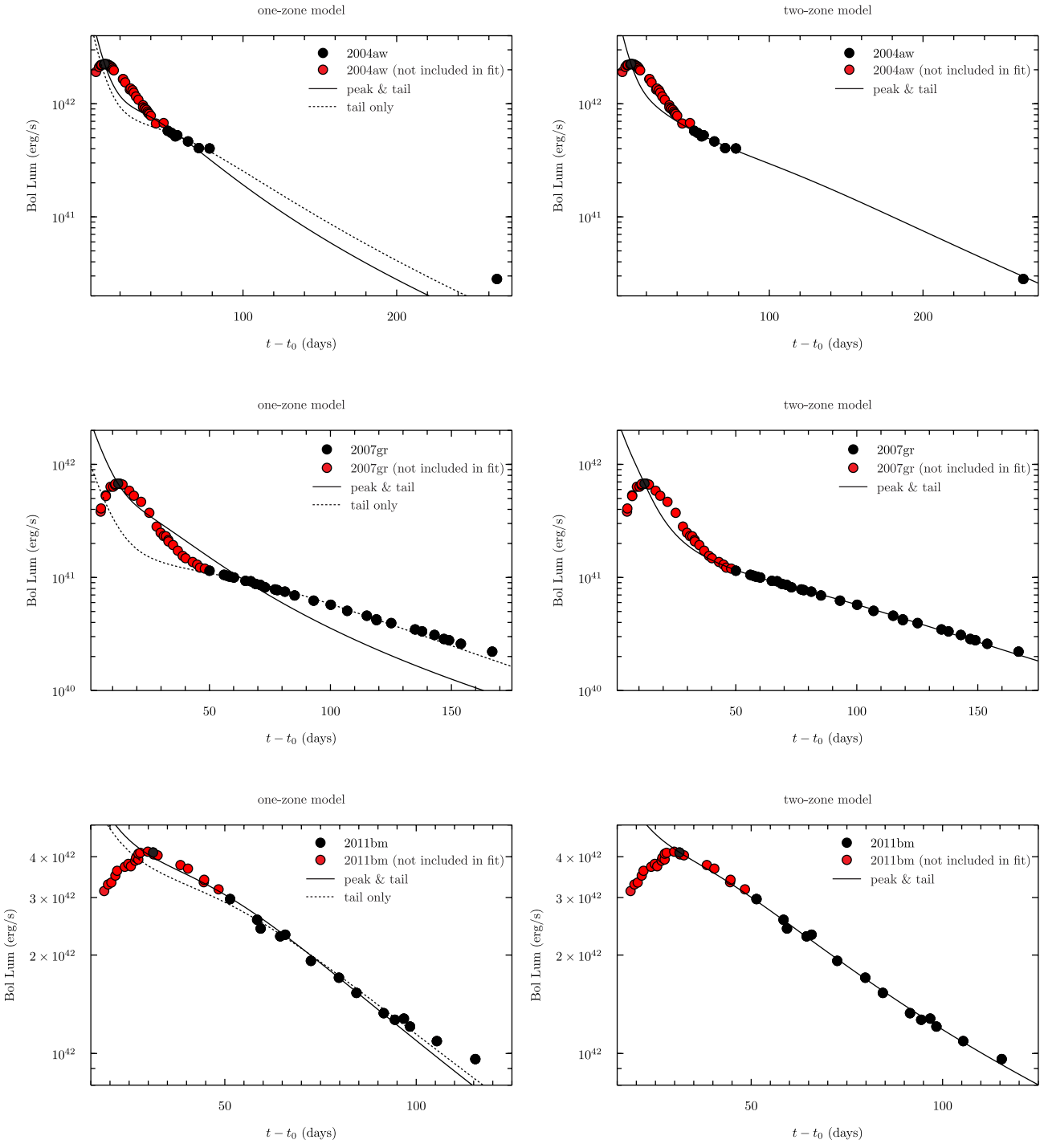

Figure 6. Bolometric LCs of the SNe Ic in our sample (2004aw, SN 2007gr and SN 2011bm). The LCs and models are displayed in the same fashion as Figs 4 and 5, with the one-zone models on the left and the two-zone models on the right. The results shown are for times >50 d. *Top:* SN 2004aw. The best-fitting model is the one-zone model. *Middle:* SN 2007gr. The one-zone model (peak+tail) is a poor visual fit to the tail. Instead, the best-fitting model is the two-zone model, which estimates that roughly 2–3 times more nickel is found in the outer layers of the ejecta. This result implies that the lack of helium spectral lines cannot be attributed to poor mixing in the ejecta. *Bottom:* SN 2011bm. The best-fitting model is the one-zone model. The one-zone model provides a better fit to the bolometric LCs of two of the three SNe Ic considered in this paper, and the best-fitting parameters determined from both models are displayed in Table 1.

ACKNOWLEDGEMENTS

We would like to thank P. Jakobsson, G. Leloudas and the anonymous referee for their excellent comments and suggestions on the original manuscript. ZC gratefully acknowledges support from a Project Grant from the Icelandic Research Fund. SS acknowledges support from the Iniciativa Cientifica Milenio grant P10-064-F (Millennium Center for Supernova Science), with input from 'Fondo de Innovación para la Competitividad, del Ministerio de Economía, Fomento y Turismo de Chile', and Basal-CATA (PFB-06/2007). The work by KM is partly supported by Grant-in-Aid for Scientific

Research of JSPS (23740141), and by World Premier International Research Center Initiative (WPI Initiative), MEXT, Japan.

REFERENCES

Ade P. A. R. et al. (Planck Collaboration), 2013, preprint (arXiv:1303.5076)
Arnett W. D., 1982, ApJ, 253, 785
Benetti S. et al., 2011, MNRAS, 411, 2726
Bersten M. C. et al., 2012, ApJ, 757, 31
Branch D. et al., 2002, ApJ, 566, 1005
Cano Z., 2013, MNRAS, 434, 1098
Cano Z. et al., 2011, ApJ, 740, 41
Clocchiatti A., Wheeler J. C., 1997, ApJ, 491, 375
Clocchiatti A., Wheeler J. C., Brotherton M. S., Cochran A. L., Wills D., Barker E. S., Turatto M., 1996, ApJ, 462, 462
Clocchiatti A., Leibundgut B., Spyromilio J., Benetti S., Cappellaro E., Turatto M., Phillips M. M., 2004, in Hoflich P., Kumar P., Wheeler J. C., eds, Cosmic Explosions in Three Dimensions. Cambridge Univ. Press, Cambridge, p. 50
Deng J. S., Qiu Y. L., Hu J. Y., Hatano K., Branch D., 2000, ApJ, 540, 452
Dessart L., Hillier D. J., Livne E., Yoon S.-C., Woosley S., Waldman R., Langer N., 2011, MNRAS, 414, 2985 (D12)
Dessart L., Hillier D. J., Li C., Woosley S., 2012, MNRAS, 424, 2139
Eldridge J. J., Fraser M., Smartt S. J., Maund J. R., Crockett R. M., 2013, MNRAS, 436, 774
Ensman L. M., Woosley S. E., 1988, ApJ, 333, 754
Falco E. E. et al., 1999, PASP, 111, 438
Filippenko A. V., 1997, ARA&A, 35, 309
Filippenko A. V. et al., 1995, ApJ, 450, L11
Frey L. H., Fryer C. L., Young P. A., 2013, ApJ, 773, L7
Fukugita M., Shimasaku K., Ichikawa T., 1995, PASP, 107, 945
Gerardy C. L., Marion G. H., Fesen R. A., Höflich P., Wheeler J. C., Nomoto K., Motohara K., 2002, BAAS, 34, 1204
Hachinger S., Mazzali P. A., Taubenberger S., Hillebrandt W., Nomoto K., Sauer D. N., 2012, MNRAS, 422, 70
Harkness R. P. et al., 1987, ApJ, 317, 355
Hunter D. J. et al., 2009, A&A, 508, 371
Leibundgut B., Suntzeff N. B., 2003, in Weiler K., ed., Lecture Notes in Physics, Vol. 598, Supernovae and Gamma-Ray Bursters. Springer-Verlag, Berlin, p. 77
Li H., McCray R., 1995, ApJ, 441, 821
Li C., Hillier D. J., Dessart L., 2012, MNRAS, 426, 1671
Lucy L. B., 1991, ApJ, 383, 308
Maeda K., Nomoto K., 2003, ApJ, 598, 1163
Maeda K., Mazzali P. A., Deng J., Nomoto K., Yoshii Y., Tomita H., Kobayashi Y., 2003, ApJ, 593, 931 (M03)
Maeda K. et al., 2008, Science, 319, 1220
Malesani D. et al., 2009, ApJ, 692, L84
Matheson T., Filippenko A. V., Li W., Leonard D. C., Shields J. C., 2001, AJ, 121, 1648
Mazzali P. A., Lucy L. B., 1998, MNRAS, 295, 428
Millard J. et al., 1999, ApJ, 527, 746
Modjaz M., Kirshner R. P., Blondin S., Challis P., Matheson T., 2008, ApJ, 687, L9
Modjaz M. et al., 2009, ApJ, 702, 226
Moriya T., Tominaga N., Tanaka M., Maeda K., Nomoto K., 2010, ApJ, 717, L83
Panagia N., Gilmozzi R., Macchetto F., Adorf H.-M., Kirshner R. P., 1991, ApJ, 380, L23
Piro A. L., Nakar E., 2013, ApJ, 769, 67
Podsiadlowski P., Joss P. C., Hsu J. J. L., 1992, ApJ, 391, 246
Sana H. et al., 2012, Science, 337, 444
Smartt S. J., 2009, ARA&A, 47, 63
Stritzinger M. et al., 2009, ApJ, 696, 713
Swartz D. A., Filippenko A. V., Nomoto K., Wheeler J. C., 1993, ApJ, 411, 313
Takaki K. et al., 2013, ApJ, 772, L17
Taubenberger S. et al., 2006, MNRAS, 371, 1459
Taubenberger S. et al., 2009, MNRAS, 397, 677
Thomas R. C., Nugent P. E., Meza J. C., 2011, PASP, 123, 237
Tomita H. et al., 2006, ApJ, 644, 400
Valenti S. et al., 2008, ApJ, 673, L155
Valenti S. et al., 2011, MNRAS, 416, 3138
Valenti S. et al., 2012, ApJ, 749, L28
Wheeler J. C., Harkness R. P., Clocchiatti A., Benetti S., Brotherton M. S., Depoy D. L., Elias J., 1994, ApJ, 436, L135
Woosley S. E., Langer N., Weaver T. A., 1995, ApJ, 448, 315
Yaron O., Gal-Yam A., 2012, PASP, 124, 668

This paper has been typeset from a TEX/LATEX file prepared by the author.